

A Fully Automatic Tool for Counting Virchow-Robin Spaces in Magnetic Resonance Imaging for Lacunar Stroke Study

Sérgio Pereira¹, José A. Mariz², Nuno Sousa², José H. Correia¹ and Carlos A. Silva¹

¹Electronics Department, University of Minho, Campus Azurém, Guimarães, Portugal

²Life and Health Science Research Institute (ICVS), School of Health Sciences, University of Minho, Portugal and ICVS/3B's - PT Government Associate Laboratory, Braga/Guimarães, Portugal

Keywords: Virchow-Robin Spaces, Lacunar Stroke, MRI, Medical Image Analysis, Automatic Tool.

Abstract: Virchow-Robin Spaces surround the perforating arteries of the brain and sometimes they become dilated. Studies suggest that those structures are correlated with some conditions such as lacunar strokes, small vessel diseases, multiple sclerosis or even normal aging. However, the majority of those studies are based on the detection of those structures by a human expert, in some regions of interest, which is prone to the subjectivity of the person doing the task. Moreover, dilated Virchow-Robin Spaces may look similar to lacunar strokes, making them difficult to identify. Few works have been proposed on the computational detection of dilated Virchow-Robin Spaces. In this paper, we propose a fully automatic tool, capable of preprocessing the magnetic resonance images, extract the most relevant regions of interest and detect dilated Virchow-Robin Spaces. Such a tool may be useful to eliminate human subjectivity, but also to improve the reproducibility of the studies, leading to more reliable correlations. An application to visualize and count the detected structures was also built, with the aim of helping in a study of the correlation of lacunar strokes, Virchow-Robin Spaces and vascular dementia.

1 INTRODUCTION

Virchow-Robin Spaces (VRS) are the spaces, filled with cerebrospinal fluid (CSF) and interstitial fluid, between the perforating arteries of the brain and an extension of the pia mater that surrounds the blood vessel (Rouhl et al., 2008). Typically, VRS are microscopic structures, but they can become dilated, which makes them visible in magnetic resonance imaging (MRI), with intensity near the CSF. However, the dimensions of dilated VRS are, usually, between 3 mm and 15 mm for its length and up to 3 mm in diameter (Descombes et al., 2004), which is near the resolution of the MRI scanners. So, the identification of these structures is difficult not only for computational methods, but also for physicians. In fact, they may be mistakenly identified as lacunar strokes (Hernández et al., 2013).

The importance of detecting dilated VRS is related with studies that suggest that there is a correlation between the number of these structures and some diseases or conditions, such as lacunar strokes and other small vessel diseases (Doubal et al., 2010; Rouhl et al., 2008); it can, also, be useful to distinguish vascular dementia from Alzheimer's Disease

(Patankar et al., 2005). Additionally, it was found a correlation between multiple sclerosis and the volume of dilated VRS, but not with its number (Wuerfel et al., 2008). Those studies divided dilated VRS into the regions where they were observed, being the most common, and most relevant for the studies, the basal ganglia and cerebral white matter (WM) (Patankar et al., 2005; Doubal et al., 2010; Rouhl et al., 2008). However, dilated VRS are also observed in healthy elderly people and, although less frequently, in younger people, which makes some authors to argue that it is just a feature of normal aging (Groeschel et al., 2006).

There are few works dedicated to computational methods for the detection of dilated VRS. In (Descombes et al., 2004), the authors proposed an automatic method by modeling the geometry and spatial distribution of dilated VRS with a Marked Point Process, that was, then, optimized with a Reversible Jump Markov Chain Monte Carlo (RJCMCMC) algorithm and simulated annealing, using the T1-weighted MPRAGE sequence. Other authors applied a multi-sequence approach with thresholds and connected regions, but it had the disadvantage of being semiautomatic (Wuerfel et al., 2008). It is difficult to differentiate lacunar infarcts from VRS, even for specialists,

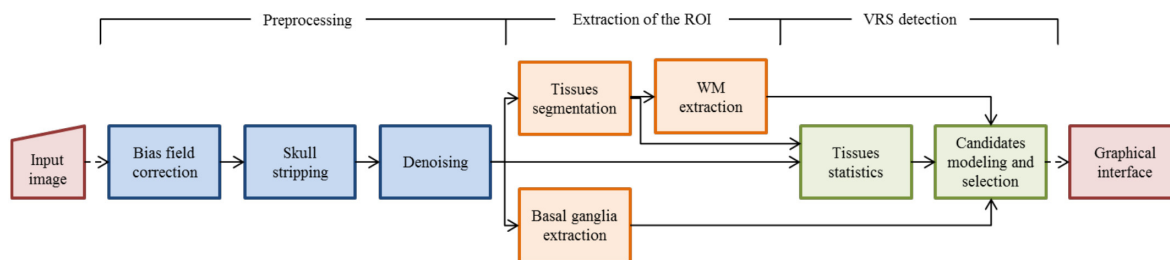


Figure 1: Proposed pipeline.

so in (Uchiyama et al., 2008) it was proposed an automatic method that extracted both, and then identified VRS with a neural network classifier. Other times dilated VRS were treated as false positives, such as in (Ramirez et al., 2011), where the objective was to segment subcortical hyperintensities with an adaptive threshold, and after that VRS were removed by deleting small connected components.

A recent review on automatic assessment of dilated VRS (Hernández et al., 2013) concluded that there are too few methods. It is pointed out that a successful method would be multi-sequence, and it should detect dilated VRS for different brain regions, taking into account the intensity, shape, size, location and spatial distribution. We believe that given the clinical attention those structures are receiving, a method for the automatic detection of dilated VRS would be important, since it would lead to more reproducible evaluation and more meaningful results.

In this paper, we propose a complete and fully automatic tool for the detection of dilated VRS, using MRI, in two specific brain regions, the basal ganglia and cerebral WM. The aim of the proposed tool is for supporting a study on lacunar strokes and its correlation with dementia. The pipeline comprises several procedures, namely the correction of the bias field, skull stripping, extraction of regions of interest and detection of dilated VRS. Finally, it was, also, developed an application to display the counting and to facilitate the analysis of the detected dilated VRS.

The remainder of this paper is organized as follows. In Section 2, we present the stages of the pipeline and the main features of the graphical application. We discuss results and show some images of detected VRS and the graphical application in Section 3. Finally, we summarize the main contributions and identify future developments in Section 4.

2 METHODS

The proposed tool has three main stages: preprocessing, extraction of the region of interest (ROI) of the brain, and detection and counting of dilated VRS.

Also, a graphical user interface was developed to permit the visualization and inspection of the detected structures (Figure 4). Figure 1 depicts the proposed pipeline. Each stage comprises the execution of several algorithms, whose implementation is found in public neuroimaging packages or in-house solutions. These commands are integrated in the pipeline using the software package Nipype (Gorgolewski et al., 2011), allowing their automatic execution.

2.1 Preprocessing

Since our goal was to obtain an automatic tool that could be applied right after the acquisition of the images, the first stage aims to prepare the acquired images for segmentation.

We start by correcting the bias field with the N4ITK method (Tustison et al., 2010), which ensures that the intensity of the same type of tissues stays uniform along the brain. This is important because we use the intensities of the tissues to build filters, analyze VRS candidates and segment WM and gray matter (GM), in a further stage. After evaluating other alternatives, we opted for the skull stripping procedure distributed with Freesurfer (Ségonne et al., 2004); this step is important for our tissue segmentation method. As the last step in the preprocessing stage, we denoise the image, since noise increases the false detection of dilated VRS. We selected the rotationally invariant

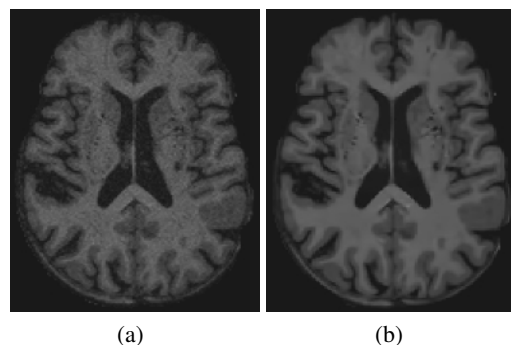


Figure 2: Effect of denoising. In a) can be observed the original image, before denoising; the resulting image, without noise is in b).

nonlocal means filter (Manjón et al., 2012), which in our tests preserved better the fine details and had less smoothing, which could compromise the detection of dilated VRS, as can be observed in Figure 2.

2.2 Extraction of the Regions of Interest

In this stage, the basal ganglia and cerebral WM are extracted.

2.2.1 Basal Ganglia

Basal ganglia comprises the caudate nucleus, putamen and globus pallidus. This region together with the brainstem was segmented with the subcortical segmentation method included in Freesurfer (Fischl et al., 2002). The reason for the inclusion of the brainstem is that it contains substantia nigra, which is an important region with penetrating arteries. However, this ROI is commonly affected by strokes and microbleeds that sometimes result in holes in the segmentation. To cope with the incorrect segmentation, we apply the dilation morphological operator to close the holes. This dilation permits, also, to extend the segmentation to include the subinsular region, which is an important region for dilated VRS. The basal ganglia of one subject in the axial plane, before and after correction, can be observed in Figure 3.

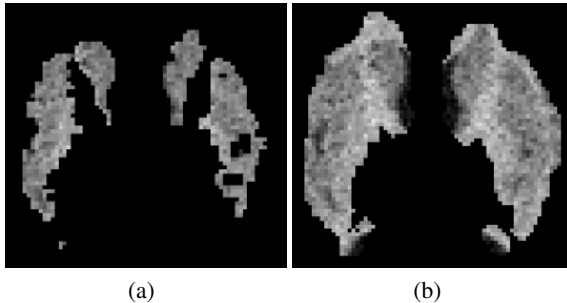


Figure 3: Basal ganglia segmented by freesurfer (a) and after correction (b).

2.2.2 Cerebral White Matter

To extract the cerebral WM, it was applied a method developed in-house (Pereira et al., 2013) to segment the brain into CSF, GM and WM. This segmentation is performed by classifying each voxel according to the tissue type. The classifier is a Random Forest, which exhibits important properties as being a multi-class classifier and having good generalization capabilities for unseen data. Also, it is capable to handle large feature vectors without overfitting, which permits good characterization of the problem. As features, we used the intensity of the voxel, measures

(mean, sum and median) in the axial plane centered in the voxel under analysis with areas of 3, 9, 15 and 19 mm², tissues posterior probabilities, tissues probability maps and the magnitude of the gradient.

As the segmentation is performed by classifying each voxel individually, we may obtain isolated misclassified voxels. These are found and replaced by the mode of the neighborhood. Finally, the subcortical segmentation obtained using Freesurfer is used to remove the cerebellum and brainstem.

2.3 Detection of Dilated Virchow-Robin Spaces

For detecting VRS, we propose an extension of the method proposed by Descombes *et al.* (Descombes et al., 2004), which we briefly describe below, indicating steps where we have diverged from, in our implementation.

Given the geometry of dilated VRS, Descombes modeled them as cylindrical structures with length between 3 and 15 mm and diameter between 1 and 3 mm. Since their intensity is similar to the CSF and they are surrounded by normal tissue, whose intensity is higher and contrasts with the VRS, the image is filtered in each plane with three filters. This filtering aims to enhance the voxels whose properties are similar to a VRS. The formulation of these filters are based on the mean and standard deviation of the CSF, GM and WM, which requires the segmentation of the brain in those regions. Departing from the original proposal (Descombes et al., 2004), we have used the segmentation method proposed in the previous section. The original proposal was based on a region growing method; the segmentation provided by this method has potential to be impaired by a class leaking into another region, which may require intervention from the user, while the segmentation method proposed in the pipeline is completely automatic.

The candidates obtained as output of the combined response of the filters have to be aggregated as a possible VRS. Departing from the authors, for each positive value, we have found the direction for which that response happened, and we followed it by advancing one slice in each iteration until there isn't more positive values in the 9 voxels right in front of the last that have been included; doing so, it was possible to find a starting point and the length of each candidate.

Having the candidates to dilated VRS, their geometry, interaction among them and their intensity were modeled with a Marked Point Process (Descombes et al., 2004). Each candidate, s , has a point, corresponding to the point where it starts, x , and a mark, l ,

that is a 3D vector representing the length and orientation of the candidate in each axis; so, $\mathbf{s} = (x, \mathbf{l})$.

Given a configuration of marked points (\mathbf{c}), the model, h , is composed by a prior term, f , and a data term g (Descombes et al., 2004),

$$h(\mathbf{c}) = f(\mathbf{c})g(\mathbf{c}) \quad (1)$$

The prior term models the length of the candidates and relations between them, while the data term takes into account the intensity along the candidate, as well as the intensity after each of its ending voxels.

In order to select the configuration of candidates corresponding to real dilated VRS, Descombes employed a Reversible Jump Markov Chain Monte Carlo algorithm with simulation annealing to globally optimize the model. Diverging from Descombes, who have used a geometrical cooling schedule, we have chosen to follow an exponential cooling schedule (equation (2)), as described in (Murphy, 2012), because we have found that it provided better convergence.

$$T_t = T_0 C^t, \quad (2)$$

where T_t is the temperature at iteration t , T_0 is the initial temperature, defined as $T_0 = 1$, and C is the cooling rate, defined as $C = 0.8$.

2.4 Visualization Application

In order to facilitate the observation and analysis of the detected dilated VRS, we developed a graphical application as presented in Figure 4. Common to all three panels is a section that allows the user to select the desired panel (Figure 4(a)-I). The main panel (Figure 4(a)) has a section to select the image to be loaded and the image with detected VRS. There, it is, also, possible to turn on or off the layer with the detected dilated VRS and to check the counting of the detected structures (II). In III, we present the 3D reconstruction of the selected dilated VRS in the viewers (IV) with the image of the ROI that has the detected VRS overlaid.

The application permits to visualize the 3D reconstruction of the ROI, as well as the detected VRS, as depicted in Figure 4(b) for the basal ganglia. Finally, the ROI with the detected VRS overlaid is, also, reconstructed (Figure 4(c)).

3 RESULTS AND DISCUSSION

The database used for the detection of dilated VRS was acquired at the Hospital of Braga, Portugal, from

9 elderly patients, whose mean age was 69.4, that had a clinical minor stroke within 6 months of the cerebral MRI acquisition and had at least one vascular risk factor as hypertension, diabetes or high cholesterol levels. For each of them there was available a 3D T1-weighted MPRAGE sequence (176 sagittal slices, matrix 256 X 256, 1 mm isotropic resolution, TR 2730 ms, TE 3.48 ms), acquired with a Siemens Avanto 1.5 T scanner. To segment the tissues of our MPRAGE sequence images, we used the Random Forest that was trained to participate in Grand Challenge on MR Brain Image Segmentation (MR-BrainS¹). Although the intensity range is different, the normalization procedure permitted to normalize the intensities between both databases.

3.1 Tool

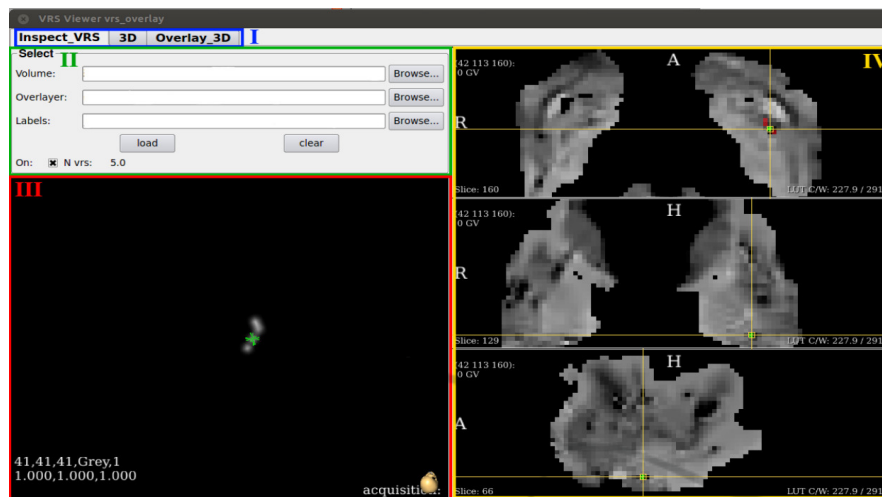
Figure 4 depicts the potential of the proposed tool. With it, physicians can easily retrieve the number of dilated VRS for each ROI, as well as inspect the scan of the subject to confirm if it presents abnormalities related to small vessel diseases, or others, which would allow a better understanding of the correlation between dilated VRS and those abnormalities. 3D reconstruction of the detected dilated VRS may be useful to provide insight into the spatial distribution of those structures, as well as if there exists any correlation between the distribution and the diseases, while 3D reconstruction of the ROI permits to confirm if it was well extracted. The 3D reconstruction of the ROI, or brain, with VRS overlaid is useful to understand if its propagation through the brain parenchyma coincide with the perforating arteries.

When the FLAIR sequence is available, the method to segment tissues is able to segment WM lesions. This potentiality makes the tool capable to measure its number and volume, which may be useful for studies that hypothesize a correlation between dilated VRS and WM lesions.

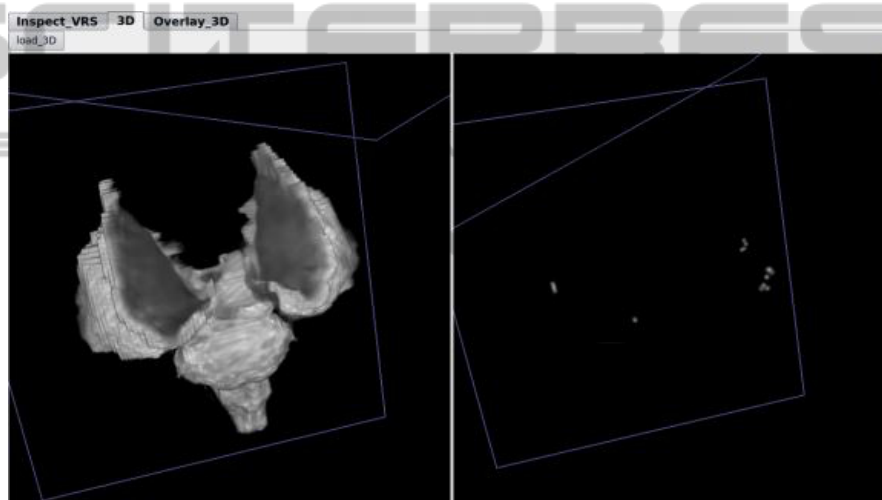
3.2 Detection of Dilated VRS

The first row of Figure 5(a) and Figure 5(b) show some examples of dilated VRS detected by the algorithm in the basal ganglia and cerebral WM, respectively. In both cases, the examples seem to have properties of dilated VRS, such as the low intensity, surrounded by normal tissue, and small size. In the second row of Figure 5(a) and Figure 5(b) is shown the 3D reconstruction of each detected VRS, which allows the physicians to observe the tortuosity; the green mark is located in the voxel that was selected

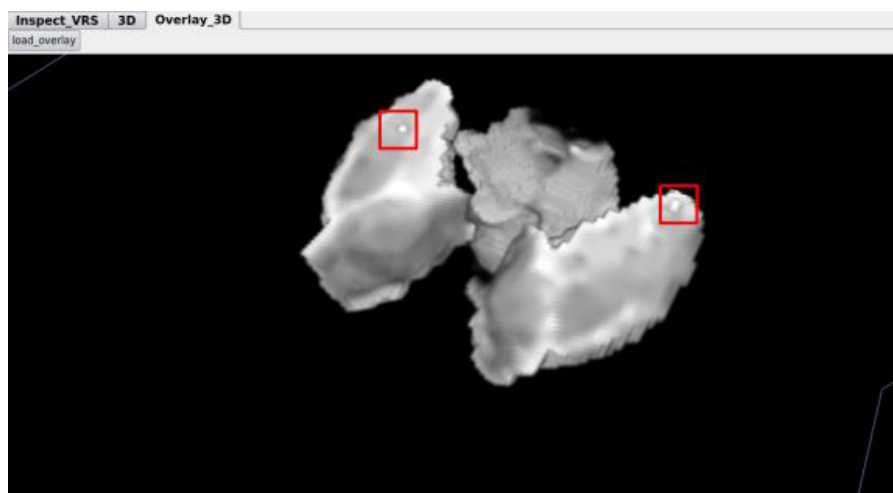
¹<http://mrbrains13.isi.uu.n>



(a)



(b)



(c)

Figure 4: Application for the visualization of the detected VRS. In a) the image of the ROI is depicted with the detected dilated VRS and its counting, b) shows the 3D reconstruction of the ROI and the detected VRS; while in c) the 3D reconstruction of the VRS overlaid over the ROI is shown.

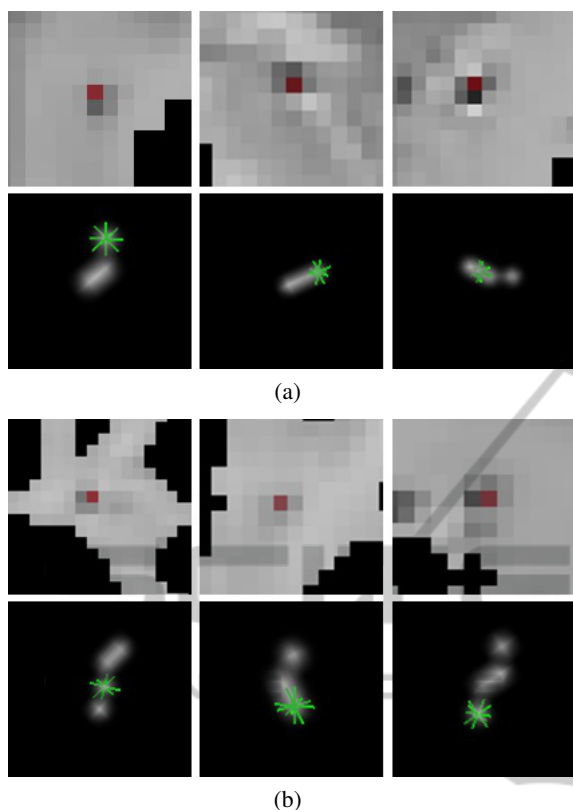


Figure 5: Examples of detected dilated VRS and their 3D reconstruction, in a) basal ganglia and b) white matter.

in the viewer, facilitating the correspondence between the reconstruction and the image by the user. In the first example of Figure 5(a) the green mark is over the first voxel of the VRS, while in the last of Figure 5(b) is over the last voxel, but in both cases it is possible to observe that the dilated VRS changes its direction.

4 CONCLUSIONS

In this paper, we have proposed a fully automatic tool to facilitate the analysis and studies on the relevance of dilated VRS as a biomarker for lacunar strokes and its association with dementia. It comprises a set of preprocessing procedures that improves the quality of the image for the problem we tackled. We have proposed alternative steps in an existing algorithm to detect the VRS as well as an in-house tissue segmentation algorithm. These modifications improve robustness of the detection of VRS in the presence of lesions and tissues atrophy. We believe this improvement in the robustness is required for a fully automatic pipeline.

A relevant feature of our tool is the possibility to extract a ROI, and to count dilated VRS only there,

which is impractical in a large scale study using human experts, as is our goal. The visualization of the detected VRS facilitates its analysis, being useful to help the physician decide if a lesion is a lacunar stroke or a VRS, when there are doubts. A tool with this features may facilitate the standardization among studies on dilated VRS as a global marker of cerebral vasculopathy and WM lesions.

ACKNOWLEDGEMENTS

We thank Joana Festa for her collaboration in the development of the visualization application.

REFERENCES

- Descombes, X., Kruggel, F., Wollny, G., and Gertz, H. J. (Feb. 2004). An object-based approach for detecting small brain lesions: application to virchow-robin spaces. *IEEE Trans. Med. Imag.*, 23(2):246–255.
- Doubal, F. N., MacLulich, A. M., Ferguson, K. J., Dennis, M. S., and Wardlaw, J. M. (2010). Enlarged perivascular spaces on mri are a feature of cerebral small vessel disease. *Stroke*, 41(3):450–454.
- Fischl, B., Salat, D. H., Busa, E., Albert, M., Dieterich, M., Haselgrove, C., van der Kouwe, A., Killiany, R., Kennedy, D., Klaveness, S., et al. (2002). Whole brain segmentation: automated labeling of neuroanatomical structures in the human brain. *Neuron*, 33(3):341–355.
- Gorgolewski, K., Burns, C. D., Madison, C., Clark, D., Halchenko, Y. O., Waskom, M. L., and Ghosh, S. S. (2011). Nipype: a flexible, lightweight and extensible neuroimaging data processing framework in python. *Front Neuroinform*, 5.
- Groeschel, S., Chong, W. K., Surtees, R., and Hanefeld, F. (2006). Virchow-robin spaces on magnetic resonance images: normative data, their dilatation, and a review of the literature. *Neuroradiology*, 48(10):745–754.
- Hernández, M., Piper, R. J., Wang, X., Deary, I. J., and Wardlaw, J. M. (2013). Towards the automatic computational assessment of enlarged perivascular spaces on brain magnetic resonance images: A systematic review. *JMRI - J Magn Reson Im*, 38(4):774–785.
- Manjón, J. V., Coupé, P., Buades, A., Louis Collins, D., and Robles, M. (2012). New methods for mri denoising based on sparseness and self-similarity. *Med. Image Anal.*, 16(1):18–27.
- Murphy, K. P. (2012). *Machine learning: a probabilistic perspective*. MIT Press.
- Patankar, T. F., Mitra, D., Varma, A., Snowden, J., Neary, D., and Jackson, A. (2005). Dilatation of the virchow-robin space is a sensitive indicator of cerebral microvascular disease: study in elderly patients with dementia. *AJNR Am J Neuroradiol*, 26(6):1512–1520.

- Pereira, S., Festa, J., Mariz, J. A., Sousa, N., and Silva, C. A. (2013). Automatic brain tissue segmentation of multi-sequence mr images using random decision forests. *The MIDAS Journal. In: MICCAI 2013 Workshops - The MICCAI Grand Challenge on MR Brain Image Segmentation (MRBrainS13)*.
- Ramirez, J., Gibson, E., Quddus, A., Lobaugh, N. J., Feinstein, A., Levine, B., Scott, C., Levy-Cooperman, N., Gao, F., and Black, S. E. (2011). Lesion explorer: a comprehensive segmentation and parcellation package to obtain regional volumetrics for subcortical hyperintensities and intracranial tissue. *Neuroimage*, 54(2):963–973.
- Rouhl, R., Van Oostenbrugge, R., Knottnerus, I., Staals, J., and Lodder, J. (2008). Virchow-robin spaces relate to cerebral small vessel disease severity. *J Neurol*, 255(5):692–696.
- Ségonne, F., Dale, A., Busa, E., Glessner, M., Salat, D., Hahn, H., and Fischl, B. (2004). A hybrid approach to the skull stripping problem in mri. *Neuroimage*, 22(3):1060–1075.
- Tustison, N. J., Avants, B. B., Cook, P. A., Zheng, Y., Egan, A., Yushkevich, P. A., and Gee, J. C. (April 2010). N4itk: improved n3 bias correction. *IEEE Trans. Med. Imag.*, 29(6):1310–1320.
- Uchiyama, Y., Kunieda, T., Asano, T., Kato, H., Hara, T., Kanematsu, M., Iwama, T., Hoshi, H., Kinosada, Y., and Fujita, H. (2008). Computer-aided diagnosis scheme for classification of lacunar infarcts and enlarged virchow-robin spaces in brain mr images. In *Engineering in Medicine and Biology Society, EMBC, 2008 Annual International Conference of the IEEE*, pages 3908–3911. IEEE.
- Wuerfel, J., Haertle, M., Waiczies, H., Tysiak, E., Bechmann, I., Wernecke, K. D., Zipp, F., and Paul, F. (2008). Perivascular spaces - mri marker of inflammatory activity in the brain? *Brain*, 131(9):2332–2340.